Water mass analysis of the 2018 US GEOTRACES Pacific Meridional Transect (GP15)

R. M. Lawrence [1], A. Shrikumar [1], E. Le Roy [2], J. Swift [3], P. J. Lam [4], G. Cutter [5], and K. L. Casciotti [1]

[1]Department of Earth System Science, Stanford University, Stanford, CA, USA
[2]Department of Marine Chemistry and Geochemistry, Woods Hole Oceanographic Institution, Woods Hole, MA, USA
[3]Department of Climate, Atmospheric Science, and Physical Oceanography, Scripps Institution of Oceanography, La Jolla, CA 92037, USA
[4]University of California, Santa Cruz, Department of Ocean Sciences, 1156 High St, Santa Cruz, CA 95064, USA
[5]Department of Ocean and Earth Sciences, Old Dominion University, Norfolk, VA 23529, USA

Key Points:

- We present the hydrography, nutrients, and water mass analysis results for the 2018 GEOTRACES GP15 section.
- Our modified water mass analysis methodology resulted in similar or lower residuals compared to past water mass analyses.
- These water mass analysis results will be useful tools for the interpretation of trace elements and isotopes (TEI's) along GP15.

Corresponding author: Rian Lawrence, rian@stanford.edu

Abstract

A water mass analysis is a tool for interpreting the effect of ocean mixing on the distributions of trace elements and isotopes (TEI's) along an oceanographic transect. The GEOTRACES GP15 transect along 152°W covers a wide range in latitude from Alaska to Tahiti. Our objective is to present the nutrients and hydrography of GP15 and quantify the distributions of water masses to support our understanding of TEI distributions along GP15. We used a modified Optimum Multiparameter (OMP) analysis to determine the distributions of water masses with high importance to nutrient and hydrographic features in the region. In the thermocline, our results indicated the dominance of Pacific Subarctic Upper Water (PSUW) in the subpolar gyre, Eastern North Pacific Central Water (ENPCW) in the northern subpolar gyre, and Equatorial Subsurface Water (ESSW) in the equatorial region. South Pacific Subtropical Water (SPSTW) dominated the top of the thermocline in the southern subtropical gyre, while South Pacific Central Water (SPCW) dominated the lower thermocline. Antarctic Intermediate Water (AAIW), Equatorial Intermediate Water (EqIW), and North Pacific Intermediate Water (NPIW) in the southern hemisphere, equatorial region, and northern hemisphere, respectively, occupied waters just below the thermocline. Dominant water masses in the deep waters of the southern hemisphere include Upper Circumpolar Deep Water (UCDW) and Lower Circumpolar Deep Water (LCDW) with minimal contributions from Antarctic Bottom Water (AABW). Pacific Deep Water (PDW) dominated the deep water in the northern hemisphere. Our results align well with literature descriptions of these water masses and related circulation patterns.

Plain Language Summary

This paper describes the measured water properties, such as temperature, salinity, and nutrients, and the ocean water mixing ratios derived from them, at depths sampled on a line between Alaska and Tahiti. We identified the water masses containing distinctive water properties found in this geographic area. Properties of these water masses were used to determine the theoretical contributions of each water mass to our ocean water samples. Using this information, we can determine if chemical concentrations and forms found in each sample can be explained by water mixing alone, or if additional chemical changes have occurred. Our water mass mixing results illustrate where nutrients have been regenerated in the water column, and largely align with past studies' results; however, our error is lower than in some past studies.

1 Introduction

Expected trace element and isotope (TEI) distributions from water mass mixing are determined via a water mass analysis. For example, Roshan and Wu (2015) identified water mass mixing, rather than another process such as regeneration, as the primary modulator of North Atlantic zinc distributions based on the water mass analysis results of Jenkins et al. (2015). Evans et al. (2020) used their water mass analysis results to investigate the Eastern Tropical North Pacific, an area of interest due to its oxygen deficient zone. Their results showed the secondary nitrite maximum is confined to a water mass with an oxygen concentration so low nitrate becomes the primary oxidant. They also compared distributions of iodine species to their water mass analysis results to identify possible water masses sources of redox species besides nitrite (Evans et al., 2020). Peters, Lam, and Casciotti (2018) used the water mass results of Peters, Jenkins, et al. (2018) to calculate the expected nitrate (NO_3^-) concentration and its isotopic composition of the cruise samples. This calculated expected nitrate was compared to the actual cruise measurements to estimate how much nitrate regeneration occurred to make up for any discrepancy. In sum, results from water mass analyses have proven helpful for the interpretation of many TEI's (Le Roy et al., 2018; Artigue et al., 2021; Deng et al., 2018).

The 2018 GEOTRACES GP15 transect followed 152°W from Alaska to Tahiti; a transect carefully planned by the GEOTRACES program to optimize its relevance to understanding the sources, sinks, and internal cycling of TEI's (GEOTRACES Science Planning Group, 2006). The distribution of TEI's on GP15 are thought to be influenced by the Aleutian margin, hydrothermal plumes, oxygen deficient zones (ODZ's), and differing surface ocean biogeography. The Aleutian margin is a possible boundary source of elements such as iron, silicate, and rare earth elements while likely also a boundary sink with high rates of particle scavenging in its deep waters (Lam et al., 2006; Hu et al., 2014; Hautala & Hammond, 2020; Haley et al., 2014, 2014). GP15 is also impacted by hydrothermal plumes, namely the East Pacific Rise (EPR), Loihi Seamount, and Juan de Fuca Ridge (JdFR) (Mahoney et al., 1994; Sedwick et al., 1992; Trefry et al., 1994). These are sources of trace elements; for example, the Loihi Seamount is a significant source of iron in the North Pacific (Jenkins et al., 2020). Signals from the the oxygen deficient zone of the Eastern Tropical Pacific are also seen along GP15. ODZ's are generally known to be a sink of fixed nitrogen, a source of nitrous oxide, and have characteristic nutrient and trace metal characteristics (Chang et al., 2012; Yamagishi et al., 2007; Nameroff et al., 2002). Volcanic strata surrounds the Pacific basin (the "ring of fire"), and TEI's released from the strata may be tracked by neodymium isotopes (Amakawa et al., 2004).

In addition these features, the transect also covers a wide range in surface biological regimes. GP15 transits the high-nutrient, low-chlorophyll (HNLC) conditions in the eastern subarctic Pacific, passes through the oligotrophic North Pacific subtropical gyre, crosses the HNLC conditions at the equator, and ends in some of the most oligotrophic waters in the world's oceans in the South Pacific gyre. Circulation features traversed include the Alaskan Gyre, the Pacific subtropical gyres, and the complex Pacific equatorial current system (Talley, 2011). GP15 also transects the ocean's oldest deep waters with low oxygen and high levels of regenerated nutrients (Hautala & Hammond, 2020; Holzer et al., 2021). TEI's can be compared across these regimes to better constrain uptake, scavenging, export, and regeneration. GP15 adds to GEOTRACES' growing network of basin-scale transects and contributes towards GEOTRACES's objectives of documenting TEI's and understanding TEI's physical and biological controls (Measures et al., 2007; GEOTRACES Science Planning Group, 2006). Here we describe the nutrients and hydrography measured on GP15, relating them qualitatively and quantitatively to water mass distributions in the region. A modified Optimum Multiparameter (OMP) analysis was employed to determine water mass fractions in GP15 samples (Shrikumar et al., 2022). The work presented here provides water mass and circulation context for GP15, a foundation needed to align to GEOTRACES's objectives at the basin-scale and beyond.

2 Methods

2.1 Cruise information and relevant measurements

The GEOTRACES Pacific Meridional Transect, GP15, was conducted on R/V Roger Revelle along 152°W (except for the first five stations off the coast of Alaska) from 18 September to 24 November 2018. The Oceanographic Data Facility (ODF, Scripps Institution of Oceanography) collected temperature, and salinity, dissolved oxygen, and nutrient measurements using standard methods described in the GP15 cruise report and GO-SHIP best practices (Cutter et al., 2018; Becker et al., 2020). Briefly, nitrate (μmol kg^{-1}), silicate (μmol kg^{-1}), and phosphate (μmol kg^{-1}) concentrations were measured on board after allowing sample bottles to come to room temperature over 2-12 hours. Dissolved oxygen samples were analyzed on board within 2-14 hours of collection and were also used to calibrate measurements taken via CTD sensor (Sea-Bird Electronics

9plus/ SBE9+). Data were flagged according to the SeaDataNet scheme as is recommended by GEOTRACES (SeaDataNet, 2010; GEOTRACES, n.d.). The GP15 bottle and ODF CTD data can be found on the Biological and Chemical Oceanography Data Management Office (BCO-DMO) website (Cutter et al., 2021a, 2021b, 2020) and in the 2021 GEOTRACES Intermediate Data Product (GEOTRACES Intermediate Data Product Group, 2021). Only samples from the ODF rosette, with complete data collected by ODF and without any data flagged as a known bad value were used for the analysis.

2.2 Water mass analysis

The Optimum Multiparameter (OMP) analysis was conducted using the Python package, pyompa (Shrikumar et al., 2022). pyompa contains code adapted from Peters, Jenkins, et al. (2018) and Jenkins et al. (2015). Details about the pyompa package, OMP method, and the pyompa modifications to previous implementations of the OMP method can be found in Shrikumar et al. (2022). In brief, the OMP is a system of linear equations solved via weighted least-squares for water mass fractions of each defined water type in a sample (Tomczak, 1981). Key method modifications for this GP15 implementation are discussed below. The pyompa software can be found in Zenodo (`https://zenodo.org/record/5733887`), and the code to replicate the analysis can be found in Github (`https://github.com/nitrogenlab/gp15wmascripts`).

2.2.1 Analysis structure

The water mass analysis for GP15 was divided into two analyses; one for the thermocline and the other for intermediate and deep waters. The thermocline analysis was kept separate to account for the impact of the thermocline's stratification on water mass mixing. Water masses in the thermocline were restricted to mixing along isopycnals, while the intermediate and deep water mass analysis allows some dyapycnal mixing. Details are discussed further below. Previous iterations of the OMP method also divided intermediate and deep waters into separate analyses (Jenkins et al., 2015; Peters, Jenkins, et al., 2018). The reason for this was twofold; 1) this kept deep water masses out of intermediate depths and vice versa, and 2) this increased the number of water masses that could be included while maintaining a fully-determined solution.

We were able to circumvent the first issue by implementing soft penalties (see Tables 1, 2, and Text S1). Soft penalties were set at the σ_0 and/or latitudinal limits of a water mass reported in the literature. The soft penalty penalized use of a given water mass starting at its limits, and increased the penalty the farther a sample was past the limit. This technique was used to restrict water masses to observed σ_0 ranges, as well as certain latitudes; for example, a northern water mass can be penalized from being utilized in the south.

The number of water masses used in prior analyses was constrained to be less than or equal to the number of parameters, or water mass properties, used in the analysis to obtain a fully-determined solution. By separating an oceanographic transect into regional analyses, prior studies were able to include the water masses needed to define their transect. Here, we were able to include more water masses than the number of parameters by using penalties, as described above, but also by using results of an ocean circulation model (OCIM) to constrain our results to a single solution (Holzer et al., 2021; Shrikumar et al., 2022).

The OCIM model was run with the same regional water mass definitions as the OMP analysis. The OMP was then constrained to select the solution, out of a number of equivalent solutions, that yields the water mass distribution closest to the OCIM model results. Please see Shrikumar et al. (2022) for further explanation of this method. For our OCIM-constrained OMP analysis solution, the solver did not converge on a solution for

17 of the samples. In other words, the solver didn't find a solution similar to the OCIM results with the same residuals as the unconstrained OMP analysis. However, we report solutions for these 17 samples meeting the standard residuals requirements from our OMP solver.

2.2.2 Parameters and Weighting

The properties used to define water types, as well as the sample parameters used in the analysis, included conservative temperature (℃), absolute salinity, silicate [$Si(OH)_4$] (μmol kg^{-1}), dissolved oxygen [O_2] (μmol kg^{-1}), phosphate [PO_4^{3-}] (μmol kg^{-1}), and nitrate [NO_3^-] (μmol kg^{-1}). Absolute salinity and conservative temperature data were computed from the CTD data using the Python implementation of the Gibbs Sea Water Oceanographic Toolbox of TEOS-10 (`https://teos-10.github.io/GSW-Python/`), while the other parameters were measured in sample bottles, as described above.

For the water mass analyses, we used a different set of parameter weights for the thermocline analysis than the intermediate and deep water analysis (Section 2.2.1) as in Peters, Jenkins, et al. (2018). The weights applied to the thermocline OMP analysis were 20.0, 15.5, 0.5, 5, 5, and 1 for conservative temperature, salinity, $Si(OH)_4$, NO_3^-, PO_4^{3-}, and O_2, respectively.The intermediate and deep OMP analysis weights were of 56, 80, 3, 5, 5, and 1 for conservative temperature, salinity, $Si(OH)_4$, NO_3^-, PO_4^{3-}, and O_2, respectively. See Text S2 for more details and figures S1 and S2 for a comparison to Peters, Jenkins, et al. (2018)'s cited parameter weights.

We also assessed the sensitivity of the OMP method to our chosen parameter weights using a monte carlo routine. The default weights were perturbed by up to 20% using a random number generator, 'RandomState' in python's numpy package, using fixed seed '1234.' The analysis was re-run with each set of perturbed parameter weightings (n=20). We then calculated the standard deviation of residuals resulting from the sets of perturbed parameter weighting. A low standard deviation in residuals indicates low sensitivity of results to parameter weighting.

2.2.3 Nutrient regeneration and assimilation

When fitting water mass fractions to observations from GP15, the concentrations of phosphate, oxygen, and nitrate (but not silicate) were allowed to be affected by production and remineralization of organic matter. A fixed ratio of -9.68:1 was used to relate the consumption of oxygen to the regeneration of nitrate (Broecker, 1974; Peters, Jenkins, et al., 2018), while a flexible regeneration ratio was used for oxygen to phosphate (O:P; range -96.5:1 to -305.6:1) to account for variable carbon to phosphate (C:P) ratios observed throughout the Pacific. This range in O:P was derived by assuming a $C : N : O$ ratio of 106:16:-155 (Anderson, 1995; Peters, Jenkins, et al., 2018), and varying the amount of P relative to everything else to match the upper and lower limits for C:P in the Pacific Ocean (which were 66:1 and 209:1) (Teng et al., 2014). For example, a C:P ratio of 66:1, combined with an O:C ratio of -155:106 yields an O:P ratio of -96.5:1. The solver in the OMP code finds the best fit to the observations, varying the water mass fractions and the amount of oxygen consumed or nutrients regenerated, and the ratio between changes in O_2 and changes in P needed to fit the observations (Shrikumar et al., 2022).

2.2.4 Thermocline water mass analysis

The potential density anomaly (σ_0) surfaces that defined our thermocline boundaries varied from station to station, based on the σ_0 gradient of GP15 CTD data for each station (Text S3) (Cutter et al., 2020). The upper thermocline boundary was set where either 25% of the maximum σ_0 gradient ($\frac{\partial \sigma_0}{\partial z}$) was found or where $\frac{\partial \sigma_0}{\partial z}$ reached 0.01 kg/m^4,

Table 1. Thermocline water mass definitions and penalties used in the thermocline OMP analysis. The potential density anomaly (σ_0) range is the σ_0 range of endmembers for each 0.01 kg m^{-3} increment of σ_0 available and extracted. The lowest σ_0 of the range is the lowest σ_0 at which we were able to obtain an endmember based on GLODAP v2 data for a water mass definition region (Olsen et al., 2016; Key et al., 2015; Lauvset et al., 2021). Endmembers were only extracted for $\sigma_0 \leq 27.00$ kg m^{-3}.

water mass	latitude range	longitude range	σ_0 (kg m^{-3}) range	latitude penalty	sources
SPSTSW	15°S-20°S	142°W-152°W	22.40-27.00	north of equator	Fiedler and Talley (2006)
SPCW	20°S-30°S	130°W-152°W	22.79-27.00	north of 5°N	Sprintall and Tomczak (1993)
ESSW	5°S-5°N	80°W-90°W	19.56-27.00	north of 20°N	Wyrtki (1967); Peters, Jenkins, et al. (2018)
ENPCW	16°N-26°N	170°W-140°W	21.91-27.00	south of equator	Seckel (1968); Talley (2011); Tomczak and Godfrey (2003a)
PSUW	50°N-58°N	155°W-140°W	23.71-27.00	south of 20°N	Thomson and Krassovski (2010)

Table 2. Intermediate and deep water mass definitions, number of subtypes (also referred to as a archetypes), and penalties used in the intermediate and deep water OMP analysis. The samples falling within the latitude, longitude, and potential density (σ_0) definitions of each water mass were extracted from GLODAP v2 database (Olsen et al., 2016; Key et al., 2015; Lauvset et al., 2021). An archetype analysis was then conducted to obtain water mass endmembers for the number of subtype(s) specified for a water mass.

water mass	latitude range	longitude range	σ_0 (kg m^{-3})	no. of subtypes	latitude penalty	σ_0 penalty	sources
SPCW	20°S-30°S	130°W-152°W	25.29-26.86	2	north of 5°N	≥27.4	Sprintall and Tomczak (1993)
ESSW	5°S-5°N	80°W-90°W	25.29-26.86	2	north of 20°N	≥27.2	Wyrtki (1967); Peters, Jenkins, et al. (2018)
ENPCW	16°N-26°N	170°W-140°W	25.29-26.5	2	south of equator	≥27	Seckel (1968); Talley (2011); Tomczak and Godfrey (2003a)
PSUW	50°N-58°N	155°W-140°W	25.29-26.5	2	south of 20°N	≥27.5	Thomson and Krassovski (2010)
AAIW	55°S-43°S	90°W-80°W	27.05-27.15	2	north of 10°N	≥27.6	Iudicone et al. (2007); Talley (2011); Schmitz Jr (1996)
EqIW	5°S-5°N	80°W-90°W	26.86-27.3	2	north of 20°N	≥27.2	Wyrtki (1967); Peters, Jenkins, et al. (2018); Bostock et al. (2010); Reid (1965)
NPIW	36.5°N-39°N	148°E-154°E	26.4-26.9	3	north of 10°N	none	Yasuda (1997)
UCDW	44.5°S-49.5°S	157°W-147°W	27.35-27.75	1	north of 10°N	≤27.3	Peters, Jenkins, et al. (2018); Talley (2011); Orsi et al. (1995)
LCDW	61.5°S-66.5°S	150°E-100°W	27.79-27.83	2	north of 40°N	≤27.7	Peters, Jenkins, et al. (2018); Orsi et al. (1999)
AABW	61.5°S-66.5°S	150°E-100°W	$\geq \sigma_4$ of 46.04	1	north of 30°N	≥27.6	Peters, Jenkins, et al. (2018); Orsi et al. (1999)
PDW	39°N–51°N	170°W–133°W	27.2 to σ_4 of 45.88	3	none	none	Kawabe and Fujio (2010); Haley et al. (2014); Talley (2011)

whichever was shallower. The lower bound of the thermocline was set where $\frac{\partial \sigma_0}{\partial z}$ returned to 0.003 kg/m^4. These boundaries can be seen in σ_0 and depth space in Figure S3 and resulted in 341 GP15 samples being included in the GP15 analysis.

In order to define the thermocline endmember properties, data were extracted from Global Ocean Data Analysis Project version 2 (GLODAPv2) (Olsen et al., 2016; Key et al., 2015; Lauvset et al., 2021) within the latitude, longitude, and σ_0 ranges for each thermocline water mass, described below. A cubic spline was fit to the density profile of each parameter for each water mass and used to obtain an endmember for every 0.01 kg m^{-3} increment of σ_0 (Text S4). A separate water mass analysis was then conducted for each 0.01 kg m^{-3} increment of σ_0 within each station's individual thermocline boundaries. Waters above the thermocline were not included in the analysis due to seasonal and/or annual variations in temperature, salinity, and nutrients (Fiedler & Talley, 2006; Musgrave et al., 1992; Ueno & Yasuda, 2000). However, a qualitative characterization of these surface waters is given in relation to the hydrography and nutrient distributions.

The water masses included in the thermocline OMP analysis are as follows: South Pacific Subtropical Surface Water (SPSTSW), South Pacific Central Water (SPCW), Equatorial Subsurface Water (ESSW), Eastern North Pacific Central Water (ENPCW), and Pacific Subarctic Upper Water (PSUW). Each of these water masses has a defined latitude and longitude range chosen to reflect where the waters are subducted, with preference given to proximity to the transect when subduction occurs over a large area (Table 1 and Figure 1).

SPSTSW is formed in the South Pacific Subtropical Gyre where evaporation exceeds precipitation, resulting in some of the saltiest waters found in the Pacific (Fiedler & Talley, 2006). Although it does influence the upper thermocline of the GP15 transect, it is considered a surface water mass. The geographic range we used to define this water mass was defined proximally, due to the variability in surface water salinity, and according to circulation patterns. Anything west of GP15 (152°W) was not included in the definition range given the westward flow of the South Equatorial Current (Talley, 2011).

SPCW is formed when surface waters between 155°E to 130°W in the south Pacific subtropical gyre are subducted (Sprintall & Tomczak, 1993). This water mass can be found around a σ_0 of 26.5 kg m^{-3} between 10°S and the Subantarctic Front, around 55°S (Talley, 2011). Compared to ENPCW (salinity around 35 at its shallowest reaches), SPCW is more saline (salinity around 36 at its shallowest reaches) (Emery & Meincke, 1986). The geographic range used for its origin in the literature was modified to align with the subtropical gyre's circulation (Sprintall & Tomczak, 1993; Peters, Jenkins, et al., 2018). Again, anything west of our transect (152°W) was not included in the definition range given the westward flow of the South Equatorial Current (Talley, 2011).

ESSW originates from the the west Pacific and is transported via the Equatorial Countercurrents and Undercurrents that upwell in the eastern tropical Pacific to form ESSW (Montes et al., 2014; Stramma et al., 2010). It core is fairly shallow around σ_0 of 24 to 25 kg m^{-3} (Fiedler & Talley, 2006; Silva et al., 2009). Most strongly present between 10°N and 10°S, ESSW is characterized by high temperature (7.0-23.0°C) and salinity (34.5-36.0) (Emery & Meincke, 1986; Silva et al., 2009; Wyrtki, 1967). Its salinity maximum coincides with a dissolved oxygen minimum and high nitrate and phosphate concentrations (Silva et al., 2009). The geographic range used to define ESSW in this analysis was chosen to reflect the area where the water is upwelled off the coast of South America before flowing westward along the equator as ESSW (Peters, Jenkins, et al., 2018; Wyrtki, 1967).

ENPCW is formed via surface water subduction in the north Pacific subtropical gyre between 26°N and 16°N, and its core occupies σ_0 of 25-25.8 kg m^{-3} (Seckel, 1968; Bograd et al., 2019). ENPCW is found east of 170°W and between the North Equato-

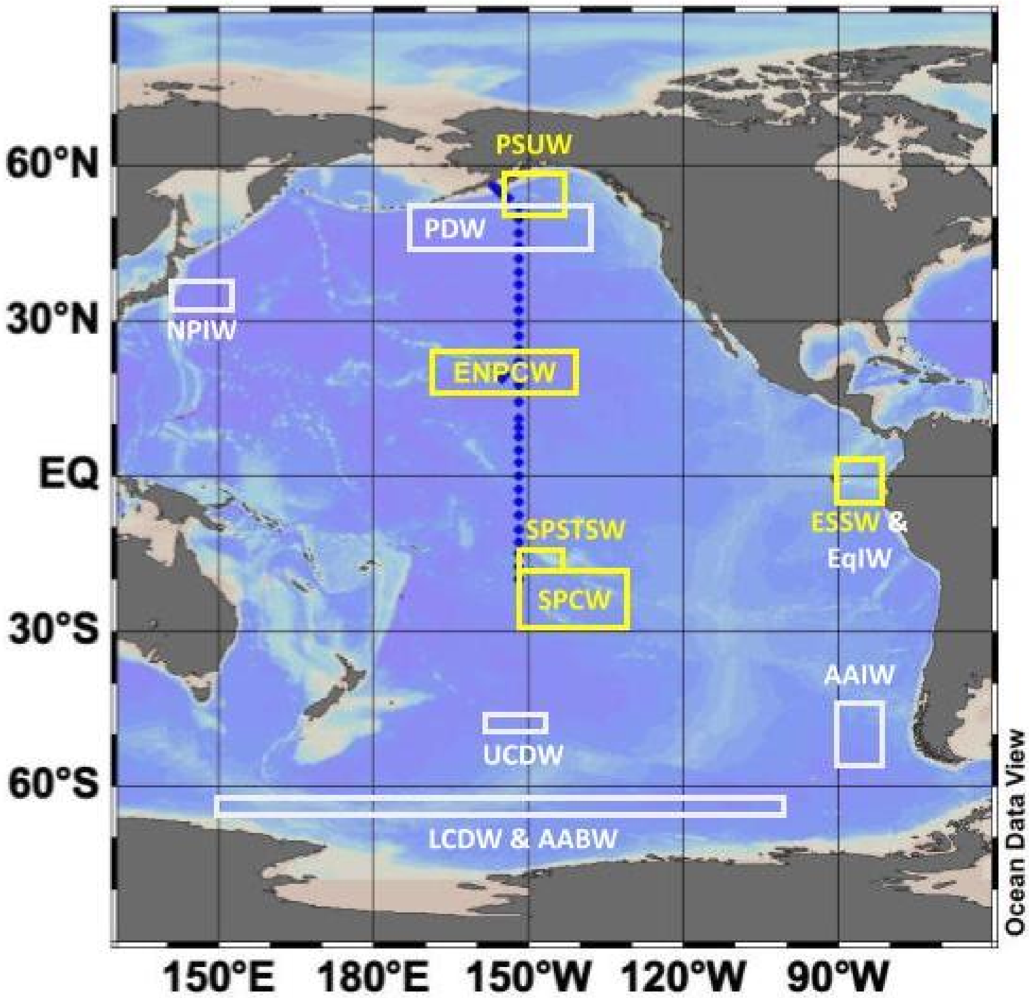

Figure 1. The latitude and longitude definition ranges for the thermocline water masses are in yellow. The ranges for the intermediate and deep waters are in white. The water mass names can be found in the 'Acronyms' section at the end of the paper.

rial Countercurrent (located 3-10°N) and 40°N (Tomczak & Godfrey, 2003b). The latitudinal range used for this analysis was defined as 16°N-26°N (Seckel, 1968). The boundary between the Eastern and Western North Pacific Central Waters according to Tomczak and Liefrink (2005) is 170°W. This serves as the western boundary of the ENPCW for our analysis while 140°W, the longitude of the California Current System, is the eastern boundary (Talley, 2011).

Cold subpolar surface waters are subducted around 50°N to form PSUW (Talley, 2011; Sverdrup et al., 1942). PSUW is typically carried east along the Subarctic Front until it hits the west coast of North America, moving south and mixing with central water (Tomczak & Godfrey, 2003b; Sverdrup et al., 1942). Its core is found between a σ_0 of 25.4 and 25.6 kg m^{-3} (Bograd et al., 2019). PSUW is characterized by relatively high oxygen (250-300 μmol m^{-1}), low temperature (3.0-15.0°C), and low salinity (32.6-33.6%) compared to the other thermocline water masses on this transect (Bograd et al., 2019; Cepeda-Morales et al., 2013; Emery & Meincke, 1986; Yuan & Talley, 1992; Tomczak & Liefrink, 2005; Schroeder et al., 2019). Large fractions of PSUW are not expected south of the Subarctic Frontal Zone, which is at approximately 42°N (Talley, 2011). The geographic range used to define PSUW in this analysis was based off the area of PSUW shown in Thomson and Krassovski (2010). Due to the variability within the Gulf of Alaska, and therefore PSUW water properties, 155°W to 140°W were chosen as the longitudinal range for this water mass (Musgrave et al., 1992).

2.2.5 Deep and intermediate water mass analysis

The water masses in the intermediate and deep water OMP analysis (682 samples) include Antarctic Intermediate Water (AAIW), Equatorial Intermediate Water (EqIW), North Pacific Intermediate Water (NPIW), Upper Circumpolar Deep Water (UCDW), Lower Circumpolar Deep Water (LCDW), Antarctic Bottom Water (AABW), and Pacific Deep Water (PDW) (Figure 1). Thermocline water masses PSUW, ENPCW, ESSW, and SPCW were also included in the intermediate and deep water OMP analysis to account for any mixing between the lower thermocline and intermediate waters. A latitude, longitude, and density range was chosen for each water mass based on its origin, or literature description of where the water mass is subducted, or its water type is defined (Table 2). The GLODAP v2 data were then extracted for these ranges (Olsen et al., 2016; Key et al., 2015; Lauvset et al., 2021). The endmember properties for each water mass, were derived from the extracted GLODAPv2 data using an archetype analysis, with some water masses including multiple subtypes (archetypes) (Table S1) (Cutler & Breiman, 1994).

An archetype analysis is used to identify the points across a multidimensional dataset that can be used to define a convex shape around the observations. In other words, the archetype analysis finds the best endmembers across the water properties of the data that, if plotted over all the water properties at once, would "encompass" the most observations. The number of archetypes used here depended on the number of archetypes needed to best describe the water mass data, with support from the literature. See Shrikumar et al. (2022) for more information on archetype analysis used to determine water mass subtypes for the OMP water mass analysis.

The latitude and longitude ranges defining thermocline water masses PSUW, ENPCW, ESSW, and SPCW were discussed in Section 2.2.4. The σ_0 ranges for these thermocline water masses used in the intermediate and deep water analysis were determined by the range in the bottom boundary of the thermocline across the section (25.29 to 26.86 kg m^{-3}; Figure S3b). This was done to capture characteristics of the bottom of the thermocline, the water most likely to mix with intermediate waters. While the full σ_0 range was used for ESSW and SPCW, the range was reduced to 25.29 to 26.5 kg m^{-3} for PSUW and ENPCW to minimize overlap with the definition of NPIW (σ_0 from 26.4 - 26.9 kg m^{-3}).

NPIW and Pacific AAIW can both be identified by salinity minima (salinities around 34) in their respective hemispheres. The NPIW is formed and influenced by the northwest Pacific subtropical gyre, Okhotsk Sea, and Alaskan Gyre (Ueno & Yasuda, 2003; You et al., 2000; Talley et al., 1991, 1995; Yasuda, 1997; Van Scoy et al., 1991). NPIW increases in salinity and decreases in oxygen along its advective path across the north Pacific (Talley, 1993). We chose an origin range from the northwest source waters (34°N to 37°N and 140°E to 153°E) (Yasuda, 1997). The σ_0 range chosen (26.5 to 27.4 kg m^{-3}) encompasses the salinity minimum typically found at a σ_0 of 26.9 kg m^{-3} (You et al., 2003). NPIW is mostly confined to the North Pacific Subtropical Gyre, south of 46°N (Talley et al., 1991; Talley, 1993).

Unlike NPIW being confined to the subtropical gyre, AAIW is present throughout the subtropical South Pacific and tropical Pacific south of 15°N-10°N (Talley, 2011, 1993). The source waters for AAIW are from the Southwest Pacific (Talley, 2011; Hartin et al., 2011; Molinelli, 1981; Piola & Georgi, 1982; Georgi, 1979; McCartney, 1977; Sloyan & Rintoul, 2001). AAIW is identified by its characteristic local salinity minimum and oxygen maximum. The salinity minimum of AAIW can be found in the σ_0 range of 27.05 to 27.15 kg m^{-3} (Talley, 2011). The latitude and longitude ranges used were 43-55°S and 80-90°W, respectively (Iudicone et al., 2007; Peters, Jenkins, et al., 2018).

Compared to AAIW, EqIW has lower oxygen and higher nutrients, temperature, and salinity (Peters, Jenkins, et al., 2018; Bostock et al., 2010, 2013). EqIW is formed in the eastern equatorial Pacific and found primarily between 15°S and 15°N (Bingham & Lukas, 1995; Wyrtki, 1967; Bostock et al., 2010). Some authors have separated EqIW into northern and southern subtypes (Bingham & Lukas, 1995; Bostock et al., 2010). The northern subtype has a double salinity minimum, while the southern subtype can be found on two σ_0 surfaces, has a single salinity minimum, and has low oxygen (Bingham & Lukas, 1995). We used a range of latitude and longitude (5°S - 5°N) that should include both subtypes and allowed the archetype analysis to define two endmembers for EqIW. While the latitude and longitude ranges used in the analysis for EqIW align with that of the thermocline water mass ESSW (Peters, Jenkins, et al., 2018; Wyrtki, 1967), the σ_0 range for EqIW (26.86 - 27.3 kg m^{-3} (Reid, 1997; Bostock et al., 2010)) places it below the thermocline.

Upper Circumpolar Deep Water (UCDW) is formed from modified PDW and moves southward on an isopycnal surface similar to PDW until it is upwelled in the Southern Ocean, south of the Antarctic Circumpolar Current (ACC) (Faure & Speer, 2012; Orsi et al., 1995). UCDW coincides with a local nutrient maximum and oxygen minimum (Whitworth III et al., 1985; Talley, 2013; Orsi et al., 1995). UCDW can be found between the Hawaiian Islands (19.89°N where PDW mixes with UCDW) and the ACC (Talley, 2011; Kawabe & Fujio, 2010). As mentioned previously in Peters, Jenkins, et al. (2018), the properties of UCDW change during transport, and it is best defined relatively far from PDW to avoid overlap between the endmember properties of UCDW and PDW (Kim et al., 2013). The origin latitude and longitude ranges used here were 45.5-49.5°S and 147-157°W, respectively (Peters, Jenkins, et al., 2018). UCDW's σ_0 ranges from 27.35 - 27.75 kg m^{-3} near the northern edge of the ACC, close to the chosen latitudinal and longitudinal ranges (Orsi et al., 1995).

PDW is formed via internal mixing and upwelling of water masses and is present throughout the Pacific Ocean (Talley, 2011). PDW flows southward primarily along the eastern boundary (Reid, 1997), carrying its low oxygen, high silicate signals. Our analysis used three subtypes, in keeping with classic definitions Talley (2011), defined within the ranges 39°N–51°N and 170°W–133°W (Kawabe & Fujio, 2010).

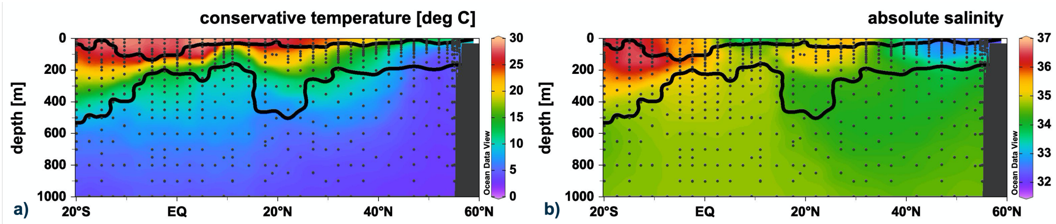

Figure 2. The panels, a) conservative temperature (°C) and b) absolute salinity, include the upper 1000 m along GP15. The black contour lines represent the upper and lower thermocline boundaries.

LCDW is identified by the vertical salinity maximum in the Antarctic Circumpolar Current (ACC) (Talley, 2011). This high salinity originates from NADW, as it enters into the ACC via the southwestern Atlantic Ocean, mixes with the circumpolar deep water, and enters the Pacific Ocean (Whitworth III et al., 1985; Orsi et al., 1995). LCDW erodes and mixes into PDW from south to north (Talley, 2011). LCDW was defined here at a latitude between 61.5 - 66.5°S, similar to earlier studies (Peters, Jenkins, et al., 2018), and longitudes between 150°E - 160°W, about width of the Pacific Ocean.

AABW is formed by deep convection at the Antarctic continental margin and does not extend much beyond 30°N in the Pacific Ocean (Orsi et al., 1999; Lee et al., 2019). AABW is found within the ACC below the circumpolar deep water. The latitude range chosen, 61.5°S to 66.5°S, was similar to prior studies (Peters, Jenkins, et al., 2018). The longitude range is about the width of the Pacific Ocean (150°E to 160°W) as AABW is found throughout the South Pacific. The σ_0 referenced to 4000 db (σ_4) for this water mass was taken as greater than 46.04 kg m^{-3} (Orsi et al., 1999).

3 Results

3.1 Temperature and salinity

The temperature and salinity distributions for GP15 reflect surface conditions, currents, and key water masses along the transect (Figure 2). In the upper 400 m between 20°S and the equator, evaporation exceeds precipitation yielding the warmest, saltiest waters of the transect (Talley, 2011). These waters primarily correspond to South Pacific Subtropical Surface Water (SPSTSW), transitioning to slightly less saline South Pacific Central Water (SPCW) through lateral and vertical mixing (Fiedler & Talley, 2006). Below the thermocline in the southern hemisphere, a salinity minimum is observed around 750 m, most strongly at 20°S (Figure 2b). This is indicative of Antarctic Intermediate Water (AAIW) (Talley, 2011; Fiedler & Talley, 2006). We also see relatively low salinity at the surface around 10°N. This is likely due to high precipitation in the Intertropical Convergence Zone (ITCZ) (Marshall et al., 2014). Underneath these low-salinity surface waters is a shoaling of cooler water, the equatorial subsurface water (Fiedler & Talley, 2006; Wyrtki, 1967).

North of 17.5°N, there is an abrupt increase in surface salinity. This marks the North Equatorial Current, separating equatorial waters from the Eastern North Pacific Central Water (ENPCW) in the North Pacific Subtropical Gyre (Talley, 2011). Salinity is higher at the surface around 25°N than in the ITCZ but lower than the southern part of the transect (Seckel, 1968; Tomczak & Godfrey, 2003a). This is likely due to higher rates of net evaporation in the South Pacific Subtropical Gyre compared to the North Pacific Subtropical Gyre (Talley, 2011). Below the ENPCW, between 200-800 m, is a salinity minimum that marks North Pacific Intermediate Water (NPIW) (Fiedler & Talley, 2006). Further north along the section, the North Pacific Current separates the Subarctic Frontal Zone and Subtropical Frontal Zone and is indicated by a large salinity gradient in the upper 200 m between 30-40°N (Figure 2b).

North of 40°N, decreasing temperature and salinity in the upper 200 m mark the presence of the Subarctic Front. Pacific Subarctic Upper Water (PSUW) is indicated by fresh, cold water seen at the surface between 40°N and the northern end of the transect (Tomczak & Godfrey, 2003a). Precipitation exceeds evaporation in the Alaskan Gyre (Royer, 1979). Coastal mountain ranges bordering the Alaskan Gyre increase the precipitation effect, and freshwater from regional glaciers, rivers, and run-off further freshen surface waters (Royer, 1979; Brown et al., 2010). We see this distinctly in the upper 50 m in the most northern part of our transect, which is evidence of the Alaskan stream (Musgrave et al., 1992).

3.2 Oxygen and nutrients

Dissolved oxygen [O_2] concentrations reflect the distributions of ventilated mode waters, low oxygen shadow zones (location of the oldest Pacific waters), and respiration during subsurface transit since a water mass last surfaced (Holzer et al., 2021). At 20°S around 550 m, relatively high O_2 (slightly higher than 200 μmol kg^{-1}) is likely Sub-Antarctic Mode Water (SAMW) (Rafter et al., 2013) (Figure 3a). Underneath is a local oxygen minimum around 1500 m from Upper Circumpolar Deep Water (UCDW) (Figure S4c) (Tomczak & Liefrink, 2005). Lower Circumpolar Deep Water (LCDW) at 20°S around 3500 m and especially Antarctic Bottom Water (AABW) around 15°S below 4000 m have higher oxygen than UCDW (Figure S4c) (Orsi et al., 1995, 1999). At 5°S and 10°N, low oxygen in the upper 200-600m are likely signals from the Peruvian oxygen deficient zone (ODZ) and Eastern Tropical North Pacific ODZ (Figure 3a). The signal is stronger in the north than the south likely due to the transect's closer proximity to the Eastern Tropical North Pacific ODZ. For many stations north of the equator, an oxygen deficit around 1000 m corresponds with high nitrate (Figure 3c) and phosphate (Figure 3d) concentrations (see Figure S4 for full depth profiles). This is a signal of PDW's accumulation of regenerated nutrients (Östlund & Stuiver, 1980; Hautala & Hammond, 2020). Around 35°N between 200 m and 400 m, O_2 is relatively high (between 200 and 250 μmol kg^{-1}). This is likely North Pacific Central Mode Water (NPCMW) (Mecking & Warner, 2001). North of 40°N, [O_2] is relatively high (260 to 307.78 μmol kg^{-1}) in the upper 150 m (Figure 3a). This oxygen feature coincides with a temperature minimum (4.54 to 14.75°C) characteristic of Dichothermal Water (DtW) (Talley, 2011; Haley et al., 2014).

Nitrate, phosphate, and silicate concentrations were all low in the upper 250 m of the subtropical gyres, reaching undetectable levels for all nutrients in the upper 100 m (Figure 3b,c,d). This matches literature expectation as the subtropical gyres are oligotrophic (Talley, 2011). Nitrate and phosphate maxima extend southward around 1500 m in UCDW (Figure S4e,f) (Tomczak & Liefrink, 2005). Relatively low phosphate and nitrate concentrations in the deepest waters in the southern part of our transect (around 3500 m at 20°S and below 4000 m between 15°S and the equator) are consistent with the presence of LCDW and AABW there (Figure S4e,f) (Orsi et al., 1995, 1999). High silicate waters were seen in the northern part of the transect, with a double silicate maximum between 2000-2500 m and 4000-5000 m around 40°N (Figure S4d) (Edmond et al., 1979; Talley & Joyce, 1992). The mid depth maximum is thought to originate from the western Pacific, while the near-bottom maximum derives from benthic fluxes in the eastern north Pacific basin (Hou et al., 2019; Hautala & Hammond, 2020).

The concentrations of nitrate and phosphate can be used to derive the distribution of N*:

$$N^* = N - 16 * P + 2.9\mu mol/kg^3 \tag{1}$$

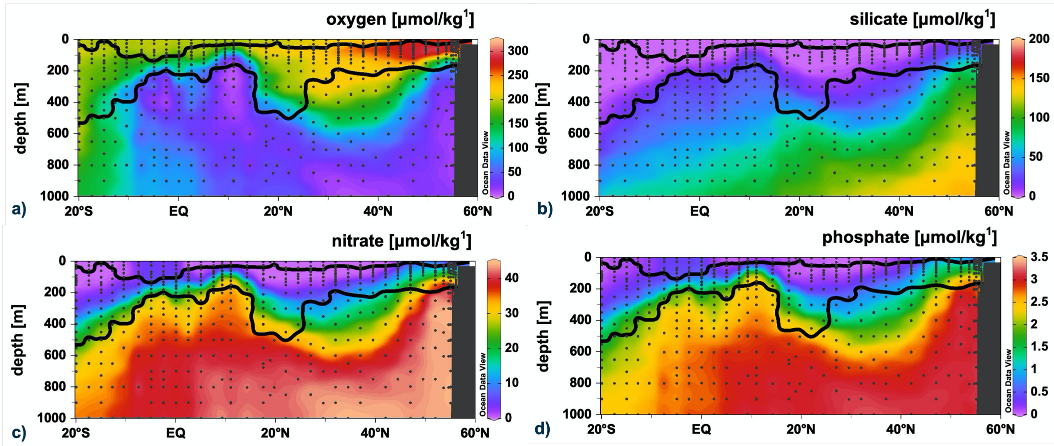

Figure 3. The panels, a) dissolved oxygen concentrations (μmol kg^{-1}), b) silicate concentrations (μmol kg^{-1}), c) nitrate concentrations (μmol kg^{-1}), and d) phosphate concentrations (μmol kg^{-1}), include the upper 1000 m of GP15. The black contour lines represent the upper and lower thermocline boundaries.

which is a measure of nitrate deficit or excess relative to phosphate (Deutsch et al., 2001). This quantity gives insights into whether nitrogen gain (via N_2 fixation) or loss (via denitrification) has occurred in a water parcel (Gruber & Sarmiento, 1997). Generally, a positive N* indicates the influence of N_2 fixation while a negative N* indicates the effects of denitrification. At 5°S and 10°N, low N* in the upper 200-600 m, coincides with low oxygen areas previously suggested to derive from the the Eastern Tropical South Pacific and Eastern Tropical North Pacific ODZs, respectively (Sarmiento, 2013). In the North Pacific Subtropical Gyre, we see low N* values (around -4) near 1000 m corresponding with the nitracline and PDW's oldest waters (Figure 4; see Figure S5 for the full water column). N_2 fixation and denitrification are typically spatially separated, with N_2 fixation occurring largely in surface waters and denitrification occurring in low-oxygen thermocline waters and shallow marine sediments. However, the lowest N* values on GP15 were found in the upper 200 m around 50°N (Figure 4), coinciding with high oxygen (Figure 3a). This could be a sedimentary denitrification signal but is somewhat separated from the shelf waters and may be imported from elsewhere (Lehmann et al., 2019). The lowest N* value flagged as "likely good" is -6.26 μmol kg^{-1} at 47°N, 41.3 dbar (Figure S6).

3.3 Thermocline boundaries

The beginning of Section 2.2.4 describes how the thermocline boundaries are defined. The upper boundary of the thermocline, which can also be called the mixed layer depth, along GP15 occurred between 20.83 kg m^{-3} and 24.63 kg m^{-3} (5.40 m - 122.39 m) (Figure S3). The boundary between the thermocline and intermediate waters occurred between 25.29 kg m^{-3} and 26.86 kg m^{-3} (85.20 m - 493.28 m). The lower boundary is relatively shallow (around 225 m) near the equator, possibly due to equatorial upwelling (Figure S3a). The σ_0 range of the thermocline is relatively wide in the subtropical gyres around 20°S and 20°N, likely due to Ekman pumping/downwelling influenced by the subtropical gyres. The thermocline boundaries are narrower in the Alaskan Gyre than the subtropical gyres, especially north of 55°N (Figure S3). The narrowing in the Alaskan Gyre may be due to Ekman upwelling, and the especially narrow boundaries around 55°N are likely due to a shallower environment on the coastal shelf of Alaska.

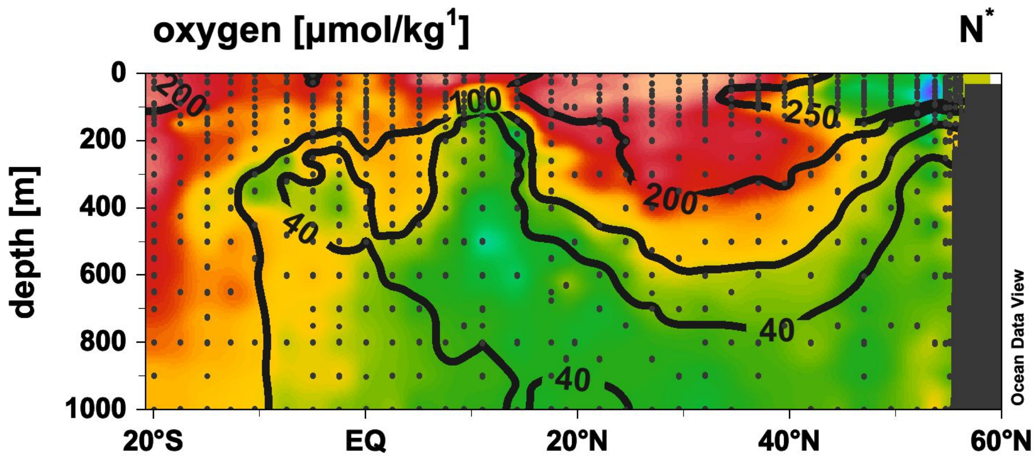

Figure 4. N* (μmol kg^{-1}) with dissolved oxygen (μmol kg^{-1}) contours in the upper 1000 m along the GP15 transect.

3.4 Phosphate regeneration and assimilation ratios

The oxygen:phosphate (O:P) ratios used to represent organic matter remineralization (or production) were allowed to vary from -96.5:1 to -305.6:1, which is derived from the range in the carbon to phosphate (C:P) ratios of organic matter observed throughout the Pacific Ocean (66:1 to 209:1) (DeVries & Deutsch, 2014; Teng et al., 2014). We can look at both the amount of regenerated (or assimilated) phosphate that is inferred by the model, as well as the O:P ratio associated with it. However, when the amount of regenerated phosphate is very small, the derived O:P ratio is not very reliable. Therefore, we restrict our interpretation of the O:P ratio to samples where regenerated (or assimilated) phosphate is greater than 0.25 umol kg^{-1} (-0.25 umol kg^{-1} for assimilation) (Figure S7).

The amount of assimilated phosphate was more than 0.25 μmol kg^{-1} only within the upper 500 m at certain latitudes along the section (Figure S7a). This quantity is negative because primary production removes phosphate from the water column relative to what would be supplied by end-member mixing. At the same time, oxygen would be produced via photosynthesis. Therefore, it make sense that assimilation would show up predominantly in the upper water column, where photosynthesis takes place. The ratio of oxygen production to phosphate assimilation was relatively low (96.5-141.8 μmol kg^{-1}), possibly due to oxygen losses to the atmosphere.

The amount of regenerated phosphate was above 0.25 μmol kg^{-1} within the upper 1500 m throughout the section (Figure S7b). Relatively high O:P ratios for regenerated phosphate were observed in the north and south subtropical gyres, while lower ratios of O:P were observed near the equator (13°S-25°N), except where the section intersects ODZ signals (Section 3.2). These observations are generally in keeping with expectations that the lowest O:P ratios (lowest C:P) would be observed in the equatorial region, and and the highest oxygen consumption O:P ratio (highest C:P) in the oligotrophic gyres (Teng et al., 2014; DeVries & Deutsch, 2014). Many of the Alaskan Gyre O:P ratios shown in Figure S7b coincide with the oldest waters of the Pacific characterized by low oxygen and high phosphate. Thus, we may not have observed low O:P ratios in the Alaskan Gyre because of pre-existing regenerated phosphate in our northern endmember.

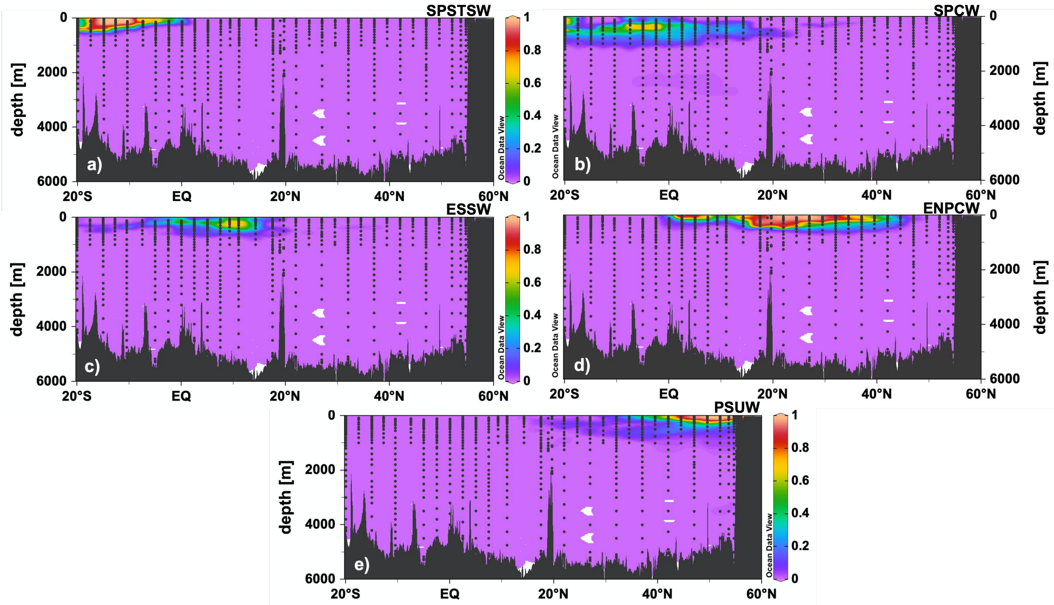

Figure 5. Thermocline water mass fractions for a) SPSTSW, b) SPCW, c) ESSW, d) ENPCW, and e) PSUW.

3.5 Distribution of Water Mass Fractions

The water mass fractions shown in figures 5 through 7 are from the OCIM-constrained OMP solution (Section 2.2.1) (Shrikumar et al., 2022). For water masses with subtypes, the individual water mass fractions for each subtype can be seen in Figure S8. SPSTSW dominated the upper thermocline between 10-15°S, and extended to the equator in lower amounts (Figure 5a) (Fiedler & Talley, 2006). Our results placed the maximum contribution of SPCW between 10°S and the equator (Figure 5b), although it extended further south to overlap its literature range (south of 10°S) (Talley, 2011). The Southern Equatorial Counter Current may have carried the relatively high fraction of SPCW to around 7°S on GP15. ESSW mixes into SPCW starting around the equator (Figure 5c). ESSW is observed between 5°N and 10°S (Emery & Meincke, 1986; Silva et al., 2009; Wyrtki, 1967), although we see higher ESSW water mass fractions north of the equator due to the subtropical gyre boundary being closer to the equator in the south than the north (Fiedler & Talley, 2006; Talley, 2011). ESSW and ENPCW mix in the lower thermocline in the tropics, reaching a maximum contribution of ENPCW around 18°N (Figure 5d). ENPCW fills the thermocline between the North Equatorial Countercurrent (located 3-10°N) and 40°N, as expected from the literature (Tomczak & Godfrey, 2003b). ENPCW begins mixing with PSUW around 40°N (Figure 5e) (Tomczak & Godfrey, 2003b; Talley, 2011). As described in the literature, the thermocline in the northernmost part of GP15 is dominated by PSUW (Sverdrup et al., 1942). Our results also reflect some water mass mixing between thermocline and intermediate waters near the bottom of the thermocline.

The highest fractions of intermediate water masses, AAIW, PEqIW, and NPIW, were found just below the thermocline, between approximately 500 m and 1250 m (Figure 6). While AAIW is described in the literature and shown in our results as primarily in the southern hemisphere, it can extend as far north as the northern subtropical gyre at approximately 10°N-15°N (Talley, 2011, 1993). Our results show low fractions of AAIW extending as far north as 20°N, aligning with its salinity minimum around 750 m depth. The highest EqIW water mass fractions were found between the equator and

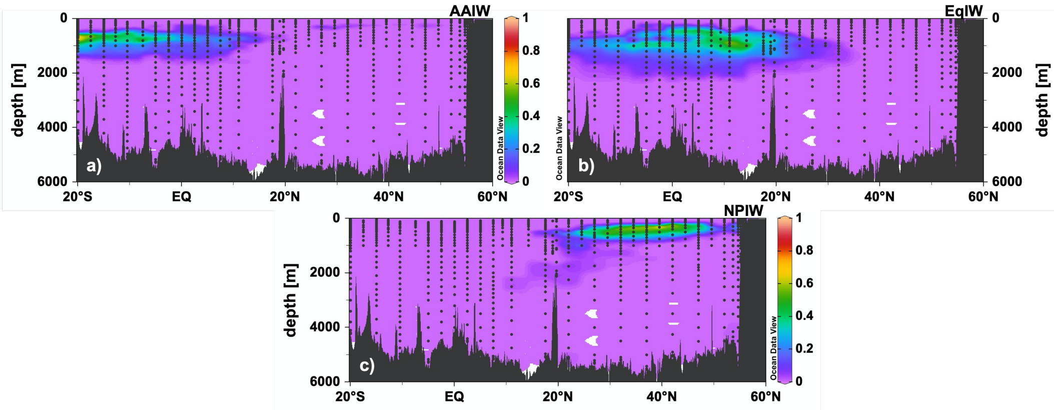

Figure 6. Intermediate water mass fractions for a) AAIW b) EqIW, and c) NPIW.

12.5°N. This falls within the literature range of between 15°S and 15°N (Reid, 1997; Silva et al., 2009; Bostock et al., 2010; Reid, 1965). The equatorial water contributing to a greater extent north of the equator may not be intuitive, but Fiedler and Talley (2006)'s placement of AAIW and NPIW leave room for EqIW just north of the equator. NPIW was mostly confined to the North Pacific Subtropical Gyre, south of 46°N, following the salinity minimum as described in the literature (Talley et al., 1991; Talley, 1993). NPIW also extended into the Alaskan Gyre, which is to be expected as the Alaskan Gyre is known to play a role in NPIW formation (You et al., 2000).

Our results confirm the presence of UCDW, LCDW, and AABW in the deep waters of the southern hemisphere. UCDW dominated depths immediately below AAIW (1000-2000 m), while LCDW was found below 2000 m (Figure 7). Upper Circumpolar Deep Water (UCDW) is found where local nutrient maxima and oxygen minima overlap as shown in Figure S9 (Whitworth III et al., 1985; Talley, 2013; Orsi et al., 1995). Lower Circumpolar Deep Water (LCDW) is primarily within the same densities as seen in Talley (2011) (Figure S10). Only small water mass fractions of AABW were present, and they were primarily confined to the deepest, southernmost part of the transect. This aligns with the literature suggesting AABW does not extend much beyond 30°N in the Pacific Ocean (Orsi et al., 1999; Lee et al., 2019). PDW dominates the deep water (approximately 1000 m and below) in the northern hemisphere, although it is found throughout the Pacific as shown by our results and the literature (Talley, 2011). PDW encompasses the oldest waters in the Pacific, and are marked by high nitrate and phosphate and low oxygen concentrations, as described in Section 3.2 (Östlund & Stuiver, 1980; Hautala & Hammond, 2020). Its highest water mass fractions also clearly follow the silicate maximums (Figure S4d).

4 Discussion

4.1 Evaluation of model performance

The standard deviation of our residuals are 0.3205℃ for temperature, 0.1079 for salinity, 2.39 μmol kg^{-1} for silicate, 0.91 μmol kg^{-1} for nitrate, 0.05 μmol kg^{-1} for phosphate, and 2.36 μmol kg^{-1} for oxygen (Figure S11). Our residuals were highest in the thermocline and showed similar patterns among most of the water properties (Figure 8). Positive residuals were generally seen in the upper 200 m around 40°N (except for conservative temperature), and negative residuals were seen in the upper 200 m around 50°N (except for conservative temperature and salinity). This pattern could be due to influence from surface waters not included in our analysis, such as those originating in the

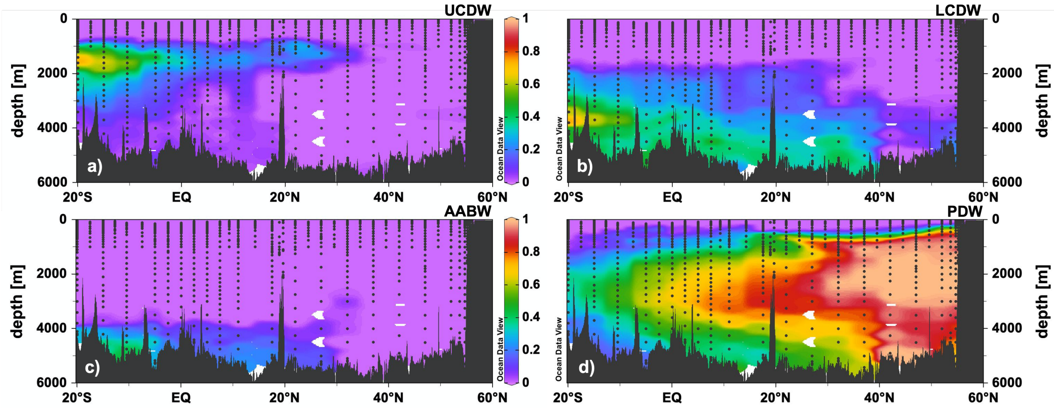

Figure 7. Deep water mass fractions for a) UCDW b) LCDW, c) AABW, and d) PDW.

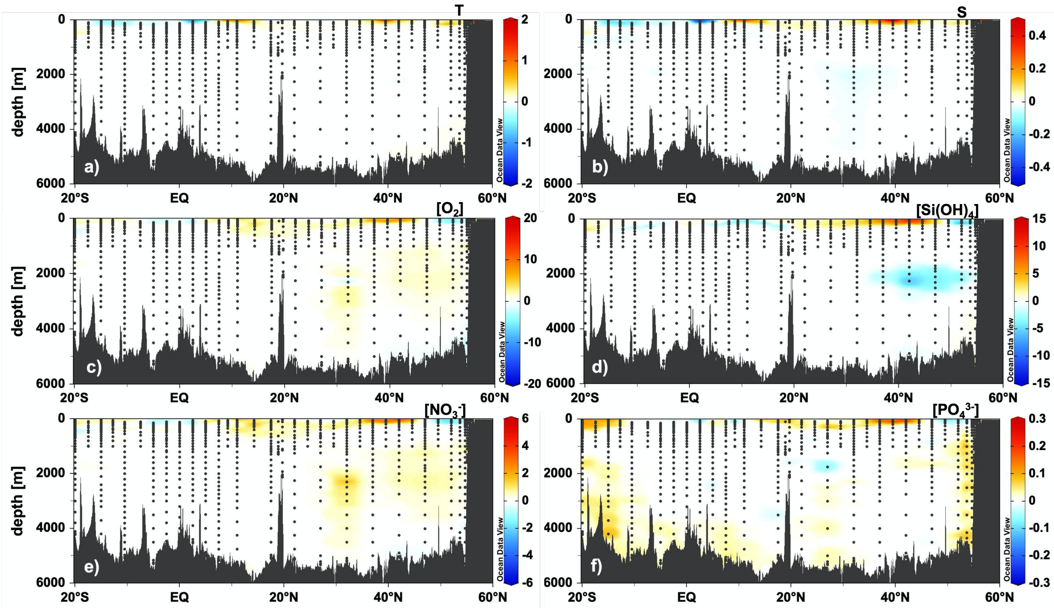

Figure 8. Residuals for a) conservative temperature (°C) b) absolute salinity, c) oxygen (μmol kg^{-1}), d) silicate (μmol kg^{-1}), e) nitrate (μmol kg^{-1}), and f) phosphate (μmol kg^{-1}).

Alaska stream, or seasonal and interannual variability in surface and near-surface waters. Relatively higher residuals in the upper water column have been observed in other OMP analyses, as these water masses are more difficult to define (Jenkins et al., 2015; Peters, Jenkins, et al., 2018; García-Ibáñez et al., 2018). Prior analyses also had higher residuals near the border separating the intermediate and deep water analyses (Peters, Jenkins, et al., 2018). One key difference in our analysis was the strictly enforced water mass conservation. In other analyses, where mass conservation is not met, residuals are generally higher for the other parameters as well (Jenkins et al., 2015; Peters, Jenkins, et al., 2018). Our average residual is 1% or less of each water property's range in GP15 measurements, comparing well with Artigue et al. (2020). A direct comparison between our residuals and the residuals of some past OMP analyses can be found in Figure S12 (García-Ibáñez et al., 2018; Peters, Jenkins, et al., 2018; Evans et al., 2020). Overall our residuals were similar to or better than other analyses.

Some of the other residuals in our analysis are informative. Between 40°N and 50°N, we see patches of relatively large (between -2 and -5 μmol kg^{-1}) silicate residuals between 2000-2500 m (Figure 8). These negative residuals indicate that the chosen water mass end members do not explain all of the silicate observed in those samples. This patch of residuals lines up with the mid-depth portion of the double silicate maximum found in the north Pacific (Edmond et al., 1979; Talley & Joyce, 1992). These residuals are likely due to either the treatment of silicate as a conservative parameter (not regenerated) or missing end members from the Bering Sea (Hautala & Hammond, 2020). Even so, these residuals are a relatively small error for silicate as 5 umol kg^{-1} corresponds to less than 3% of the range of GP15 silicate measurements.

In addition to our OMP analysis yielding low overall residuals, our solution was not sensitive to the parameter weighting chosen for the analysis. The methodology to test this was described in Section 2.2.2. The standard deviation of residuals was so low (scale of 10^{-15}) that we can conclude our OMP solution does not change significantly with up to 20% changes in parameter weightings (Figure S13).

4.2 Other water masses relevant to GP15

In addition to the water masses described above, Dichothermal water (DtW) (Talley, 2011; Haley et al., 2014) was observed on our transect, in the subpolar north Pacific at the subsurface temperature minimum and oxygen maximum (Section 3.2). These characteristics are due to its formation via subduction of cold subpolar surface waters. In the subarctic gyre, DtW was found between 80-140 m and between σ_0 26.2- 26.6 kg m^{-3} (Ueno & Yasuda, 2003; Miura et al., 2002). However, within the Alaskan Gyre, DtW was identified via elevated oxygen levels found between 30 and 100 m (Haley et al., 2014). Alaskan Gyre DtW was described to have a temperature of 3.2°C and a salinity of 32.9 (Haley et al., 2014). DtW's characteristic temperature minimum can be seen within our PSUW endmember around 26 kg m^{-3} (Figure S14). Mesothermal water (MtW) is an intermediate temperature maximum underneath DTW (Talley, 2011; Ueno & Yasuda, 2000). We did not observe MtW on GP15, however, which aligns with MtW becoming nearly undetectable by fall in the Alaskan Gyre (Ueno & Yasuda, 2000). While Haley et al. (2014) identified MtW's characteristic temperature maximum below DtW in 2007, their data were collected between August 19 - September 17, whereas our data were collected in mid-late September, 2018.

North Pacific Central Mode Water (NPCMW) was also likley observed on our transect around 35°N (Section 3.2). The WOCE transect, P16, along 152°W found NPCMW from 28-35°N and σ_0 of 26.2-26.4 kg m^{-3} (Mecking & Warner, 2001). Ladd and Thompson (2000) described the formation region of NPCMW around 40°N and 170°E to 160°W between 26.0-26.5 kg m^{-3}, while Oka and Suga (2005) describes NPCMW as being formed in the winter between 155-165°E. NPCMW has also been described to have a lighter (25.8–26.2 kg m^{-3}) version formed between the Kuroshio Extension and the Kuroshio Bifurcation fronts and a denser (26.3–26.4 kg m^{-3}) version formed farther north between the Kuroshio Bifurcation and the subarctic fronts (Oka & Suga, 2005). The properties of these versions vary year to year, as their properties depend on the adjacent front properties and locations that year. Our results find ENPCW and NPIW covering where we would expect to see NPCMW (Figure S15). This is likely due to the definitions of both ENPCMW and NPIW encompassing NPCMW, with oxygen concentrations of ENPCW around 200 μmol kg^{-1} at 26 kg m^{-3} (Figure S14) and NPIW around 268 μmol kg^{-1} (Table S1).

North Pacific Eastern Subtropical Mode Water (NPESTMW) was observed on our transect above NPCMW. It is commonly identified by a lateral minimum in potential vorticity at approximately 30°N, 140°W between σ_0 of 24.0-25.4 kg m^{-3} (Talley, 1988; Mecking & Warner, 2001). Along with an oxygen maximum, its properties include a temperature range of 16.5-22.0 °C and a salinity range of 34.0-35.4 (Hautala & Roemmich, 1998; Katsura, 2018). We likely observed the denser ESTMW (24.9 kg m^{-3}-25.2 kg m^{-3}) on our transect, rather than the lighter version (Katsura, 2018). Denser ESTMW also forms near our transect (27-35°N, 150-135°W) from deep winter mixed layers, making it more likely to impact our section. The definition of ENPCW includes NPESTMW because our ENPCW endmember properties between 24.9-25.2 kg m^{-3} are about 200 μmol kg^{-1} for O_2, 19°C for temperature, and a salinity of 35.25 (Figure S14). As on earlier occupations of line P16 (Mecking & Warner, 2001), we did not observe North Pacific Subtropical Mode Water (NPSTMW) on the GP15 transect.

Peters, Jenkins, et al. (2018) found the Peruvian ODZ signal to be carried west by the Eastern South Pacific Intermediate Water (ESPIW), which we did not include in our analysis but is likely captured by our SPCW. Indeed, the SPCW appears to capture the signal of the Peruvian ODZ, in our analysis (Figure S16), as seen around 5°S in the upper 200-600 m (Figure 3a). North of the equator, ESSW captures the signal of the Eastern North Pacific ODZ (Figure S17).

Subantarctic Mode Water (SAMW) was also likely observed on our transect via higher oxygen and low silicate (Section 3.2). As in earlier studies (Peters, Jenkins, et al., 2018), our AAIW endmember properties have some overlap with SAMW, and likely encompass it, because SAMW is difficult to distinguish from AAIW north of 20°S (Tsuchiya & Talley, 1998). This similarity can be seen in the strong similarities between our AAIW endmembers and those of Holte et al. (2013) (Table S2).

The Bering Sea (via the Kamchatka Strait) is a likely source of the high silicate concentrations characteristic of Pacific Deep Water (PDW) (Hautala & Hammond, 2020; Reed et al., 1993). To test this in our study, an alternative PDW definition was chosen from the Bering Sea around the Kamchatka Strait with latitude and longitude ranges of 55°N–60°N and 160°E–170°E, respectively. The Bering Sea water mass definition is the same as PDW in Table 2 except for the latitude and longitude ranges. The OMP was re-run with the Bering Sea water mass and all water masses previously used except for PDW. This alternate analysis eliminated the low silicate residuals (Figure S18) seen around the silicate mid depth max (2000 m at 45°N in Figure 8). However, the new residuals for oxygen and nitrate deviated farther from zero below 3000 m north of 40°N. This is likely due to the higher LCDW water mass fractions in this area (Figure S19). Phosphate residuals, primarily in the bottom 3000 m, also increased.

5 Conclusions

We observed many of the expected features from the central Pacific Ocean in this section, such as warm, salty, and oligiotrophic surface waters in the subtropical gyre, the double silicate maximum of PDW, the salinity minima of AAIW and NPIW in their respective hemispheres, and cold, fresh PSUW in the Alaska Gyre. The water mass analysis results align with earlier descriptions of the water masses and the hydrographic and nutrient features of these water masses observed on the transect. Our water mass analysis produced low residuals compared to past studies, indicating that our model describes most of GP15 sample water properties included in the analysis. These results provide a framework for the interpretation of the GEOTRACES GP15 transect data. This product will be especially useful for calculating the expected trace element and isotope (TEI) distributions from water mass mixing along GP15, if the TEI properties for each water type are known.

Acronyms

AABW Antarctic Bottom Water
AAIW Antarctic Intermediate Water
BCO-DMO Biological and Chemical Oceanography Data Management Office

ENPCW Eastern North Pacific Central Water
ESSW Equatorial Subsurface Water
EqIW Equatorial Intermediate Water
GLODAPv2 Global Ocean Data Analysis Project version 2
LCDW Lower Circumpolar Deep Water
NPIW North Pacific Intermediate Water
OCIM Ocean circulation inverse model
OMP Optimum Multiparameter
PDW Pacific Deep Water
PSUW Pacific Subarctic Upper Water
SPCW South Pacific Central Water
SPSTSW South Pacific Subtropical Surface Water
TEI Trace Elements and Isotopes
UCDW Upper Circumpolar Deep Water

Acknowledgments

The authors thank the captain and crew of R/V Revelle, the seagoing ODF Group led by S. Becker, and the GP15 supertechs C. Kelly, M. Fleisher, L. Jensen, and B. Summers for tireless and outstanding work at sea. We gratefully acknowledge the intellectual support and leadership from R. Anderson and funding from the U.S. National Science Foundation through grants OCE-1657944 to K. L. Casciotti, OCE-1658318 to P.J. Lam, and OCE-1658318 to G. Cutter. The authors declare no competing financial interests. The manuscript is prepared to comply with the AGU data policy. The datasets reported in this study can be found on the BCO-DMO website (`https://www.bco-dmo.org/dataset/778168/data`; `https://www.bco-dmo.org/dataset/777951/data`; and `https://www.bco-dmo.org/dataset/824867/data`). The pyompa software can be found in Zenodo (`https://zenodo.org/record/5733887`), and the code to replicate the analysis can be found in Github (`https://github.com/nitrogenlab/gp15wmascripts`). The results have been upload to the Stanford Digital Repository (`https://purl.stanford.edu/tv301yr5579`) and submitted to BCO-DMO.

References

Amakawa, H., Nozaki, Y., Alibo, D. S., Zhang, J., Fukugawa, K., & Nagai, H. (2004). Neodymium isotopic variations in Northwest Pacific waters. *Geochimica et Cosmochimica Acta*, *68*(4), 715–727.

Anderson, L. A. (1995). On the hydrogen and oxygen content of marine phytoplankton. *Deep Sea Research Part I: Oceanographic Research Papers*, *42*(9), 1675–1680.

Artigue, L., Lacan, F., Van Gennip, S., Lohan, M. C., Wyatt, N. J., Woodward, E. M. S., ... Drillet, Y. (2020). Water mass analysis along 22°N in the subtropical North Atlantic for the JC150 cruise (GEOTRACES, GApr08). *Deep Sea Research Part I: Oceanographic Research Papers*, *158*, 103230.

Artigue, L., Wyatt, N. J., Lacan, F., Mahaffey, C., & Lohan, M. C. (2021). The importance of water mass transport and dissolved-particle interactions on the aluminum cycle in the subtropical North Atlantic. *Global Biogeochemical Cycles*, e2020GB006569.

Becker, S., Aoyama, M., Woodward, E. M. S., Bakker, K., Coverly, S., Mahaffey, C., & Tanhua, T. (2020). GO-SHIP repeat hydrography nutrient manual: the precise and accurate determination of dissolved inorganic nutrients in seawater, using continuous flow analysis methods. *Frontiers in Marine Science*, *7*, 908.

Bingham, F. M., & Lukas, R. (1995). The distribution of intermediate water in the western equatorial Pacific during January–February 1986. *Deep Sea Research Part I: Oceanographic Research Papers*, *42*(9), 1545–1573.

Bograd, S. J., Schroeder, I. D., & Jacox, M. G. (2019). A water mass history of the Southern California current system. *Geophysical Research Letters*, *46*(12), 6690–6698.

Bostock, H. C., Opdyke, B. N., & Williams, M. J. (2010). Characterising the intermediate depth waters of the Pacific Ocean using δ13C and other geochemical tracers. *Deep Sea Research Part I: Oceanographic Research Papers*, *57*(7), 847–859.

Bostock, H. C., Sutton, P. J., Williams, M. J., & Opdyke, B. N. (2013). Reviewing the circulation and mixing of Antarctic Intermediate Water in the South Pacific using evidence from geochemical tracers and Argo float trajectories. *Deep Sea Research Part I: Oceanographic Research Papers*, *73*, 84–98.

Broecker, W. S. (1974). "NO", a conservative water-mass tracer. *Earth and Planetary Science Letters*, *23*(1), 100-107. doi: https://doi.org/10.1016/0012-821X(74)90036-3

Brown, M. T., Lippiatt, S. M., & Bruland, K. W. (2010). Dissolved aluminum, particulate aluminum, and silicic acid in northern Gulf of Alaska coastal waters: Glacial/riverine inputs and extreme reactivity. *Marine Chemistry*, *122*(1-4), 160–175.

Cepeda-Morales, J., Gaxiola-Castro, G., Beier, E., & Godínez, V. M. (2013). The mechanisms involved in defining the northern boundary of the shallow oxygen minimum zone in the eastern tropical Pacific Ocean off Mexico. *Deep Sea Research Part I: Oceanographic Research Papers*, *76*, 1–12.

Chang, B. X., Devol, A. H., & Emerson, S. R. (2012). Fixed nitrogen loss from the eastern tropical North Pacific and Arabian Sea oxygen deficient zones determined from measurements of N2: Ar. *Global Biogeochemical Cycles*, *26*(3).

Cutler, A., & Breiman, L. (1994, November). Archetypal analysis. *Technometrics*, *36*(4), 338–347.

Cutter, G. A., Casciotti, K. L., & Lam, P. J. (2018). US GEOTRACES Pacific meridional transect–GP15 cruise report.

Cutter, G. A., Casciotti, K. L., & Lam, P. J. (2020). *CTD data from the ODF rosette on the US GEOTRACES Pacific Meridional Transect (PMT) cruise (GP15) from September to November 2018.* Biological and Chemical Oceanography Data Management Office (BCO-DMO). doi: 10.26008/1912/bco-dmo.778168.2

Cutter, G. A., Casciotti, K. L., & Lam, P. J. (2021a). *Bottle file from Leg 1 (Seattle, WA to Hilo, HI) of the US GEOTRACES Pacific Meridional Transect (PMT) cruise (GP15, RR1814) on R/V Roger Revelle from September to October 2018.* Biological and Chemical Oceanography Data Management Office (BCO-DMO). doi: 10.26008/1912/bco-dmo.777951.6

Cutter, G. A., Casciotti, K. L., & Lam, P. J. (2021b). *Bottle file from Leg 2 (Hilo, HI to Papeete, French Polynesia) of the US GEOTRACES Pacific Meridional Transect (PMT) cruise (GP15, RR1815) on R/V Roger Revelle from October to November 2018.* Biological and Chemical Oceanography Data Management Office (BCO-DMO). doi: 10.26008/1912/bco-dmo.824867.5

Deng, F., Henderson, G. M., Castrillejo, M., Perez, F. F., & Steinfeldt, R. (2018). Evolution of 231 Pa and 230 Th in overflow waters of the North Atlantic. *Biogeosciences*, *15*(23), 7299–7313.

Deutsch, C., Gruber, N., Key, R. M., Sarmiento, J. L., & Ganachaud, A. (2001). Denitrification and N2 fixation in the Pacific Ocean. *Global Biogeochemical Cycles*, *15*(2), 483–506.

DeVries, T., & Deutsch, C. (2014). Large-scale variations in the stoichiometry of marine organic matter respiration. *Nature Geoscience*, *7*(12), 890–894.

Edmond, J., Jacobs, S., Gordon, A., Mantyla, A., & Weiss, R. (1979). Water column anomalies in dissolved silica over opaline pelagic sediments and the origin of the deep silica maximum. *Journal of Geophysical Research: Oceans*, *84*(C12), 7809–7826.

Emery, W., & Meincke, J. (1986). Global water masses: summary and review. *Oceanologica Acta*, *9*(4), 383–391.

Evans, N., Boles, E., Kwiecinski, J. V., Mullen, S., Wolf, M., Devol, A. H., ... Moffett, J. W. (2020). The role of water masses in shaping the distribution of redox active compounds in the Eastern Tropical North Pacific oxygen deficient zone and influencing low oxygen concentrations in the eastern Pacific Ocean. *Limnology Oceanography*, *65*(8), 1688–1705.

Faure, V., & Speer, K. (2012). Deep circulation in the eastern South Pacific Ocean. *Journal of Marine Research*, *70*(5), 748–778.

Fiedler, P. C., & Talley, L. D. (2006). Hydrography of the eastern tropical Pacific: A review. *Progress in Oceanography*, *69*(2-4), 143–180.

García-Ibáñez, M. I., Pérez, F. F., Lherminier, P., Zunino, P., Mercier, H., & Tréguer, P. (2018). Water mass distributions and transports for the 2014 GEOVIDE cruise in the North Atlantic. *Biogeosciences*, *15*(7), 2075–2090.

Georgi, D. T. (1979). Modal properties of Antarctic Intermediate Water in the southeast Pacific and the South Atlantic. *Journal of Physical Oceanography*, *9*(3), 456–468.

GEOTRACES. (n.d.). *GEOTRACES quality flag policy.* https://www.geotraces.org/geotraces-quality-flag-policy/.

GEOTRACES Intermediate Data Product Group. (2021). *The GEOTRACES Intermediate Data Product 2021 (IDP2021).* NERC EDS British Oceanographic Data Centre NOC. doi: 10.5285/cf2d9ba9-d51d-3b7c-e053-8486abc0f5fd

GEOTRACES Science Planning Group. (2006). *GEOTRACES science plan.* Scientific Committee on Oceanic Research. Baltimore, Maryland.

Gruber, N., & Sarmiento, J. L. (1997). Global patterns of marine nitrogen fixation and denitrification. *Global Biogeochemical Cycles*, *11*(2), 235–266.

Haley, B. A., Frank, M., Hathorne, E., & Pisias, N. (2014). Biogeochemical implications from dissolved rare earth element and Nd isotope distributions in the Gulf of Alaska. *Geochimica et Cosmochimica Acta*, *126*, 455–474.

Hartin, C. A., Fine, R. A., Sloyan, B. M., Talley, L. D., Chereskin, T. K., & Happell, J. (2011). Formation rates of Subantarctic mode water and Antarctic intermediate water within the South Pacific. *Deep Sea Research Part I: Oceanographic Research Papers*, *58*(5), 524–534.

Hautala, S. L., & Hammond, D. E. (2020). Abyssal pathways and the double Silica maximum in the Northeast Pacific Basin. *Geophysical Research Letters*, *47*(19), e2020GL089010.

Hautala, S. L., & Roemmich, D. H. (1998). Subtropical mode water in the Northeast Pacific Basin. *Journal of Geophysical Research: Oceans*, *103*(C6), 13055–13066.

Holte, J. W., Talley, L. D., Chereskin, T. K., & Sloyan, B. M. (2013). Subantarctic mode water in the southeast Pacific: Effect of exchange across the Subantarctic Front. *Journal of Geophysical Research: Oceans*, *118*(4), 2052–2066.

Holzer, M., DeVries, T., & de Lavergne, C. (2021). Diffusion controls the ventilation of a Pacific Shadow Zone above abyssal overturning. *Nature Communications*, *12*(1), 1–13.

Hou, Y., Hammond, D. E., Berelson, W. M., Kemnitz, N., Adkins, J. F., & Lunstrum, A. (2019). Spatial patterns of benthic silica flux in the North Pacific reflect upper ocean production. *Deep Sea Research Part I: Oceanographic Research Papers*, *148*, 25–33.

Hu, W., Chen, M., Yang, W., Zhang, R., Qiu, Y., & Zheng, M. (2014). Enhanced particle scavenging in deep water of the Aleutian Basin revealed by 210Po-

210Pb disequilibria. *Journal of Geophysical Research: Oceans*, *119*(6), 3235–3248.

Iudicone, D., Rodgers, K. B., Schopp, R., & Madec, G. (2007). An exchange window for the injection of Antarctic Intermediate Water into the South Pacific. *Journal of Physical Oceanography*, *37*(1), 31–49.

Jenkins, W., Hatta, M., Fitzsimmons, J., Schlitzer, R., Lanning, N., Shiller, A., ... others (2020). An intermediate-depth source of hydrothermal 3He and dissolved iron in the North Pacific. *Earth and Planetary Science Letters*, *539*, 116223.

Jenkins, W., Smethie Jr, W., Boyle, E., & Cutter, G. (2015). Water mass analysis for the US GEOTRACES (GA03) North Atlantic sections. *Deep Sea Research Part II: Topical Studies in Oceanography*, *116*, 6–20.

Katsura, S. (2018). Properties, formation, and dissipation of the North Pacific Eastern Subtropical Mode Water and its impact on interannual spiciness anomalies. *Progress in Oceanography*, *162*, 120–131.

Kawabe, M., & Fujio, S. (2010). Pacific Ocean circulation based on observation. *Journal of Oceanography*, *66*(3), 389–403.

Key, R. M., Olsen, A., van Heuven, S., Lauvset, S. K., Velo, A., Lin, X., ... others (2015). Global ocean data analysis project, version 2 (GLODAPv2). *ORNL/CDIAC-162, NDP-093*.

Kim, I.-N., Min, D.-H., & Macdonald, A. M. (2013). Water column denitrification rates in the oxygen minimum layer of the Pacific Ocean along 32°S. *Global Biogeochemical Cycles*, *27*(3), 816–827.

Ladd, C., & Thompson, L. A. (2000). Formation mechanisms for North Pacific central and eastern subtropical mode waters. *Journal of Physical Oceanography*, *30*(5), 868–887.

Lam, P. J., Bishop, J. K., Henning, C. C., Marcus, M. A., Waychunas, G. A., & Fung, I. Y. (2006). Wintertime phytoplankton bloom in the subarctic Pacific supported by continental margin iron. *Global Biogeochemical Cycles*, *20*(1).

Lauvset, S. K., Lange, N., Tanhua, T., Bittig, H. C., Olsen, A., Kozyr, A., ... others (2021). An updated version of the global interior ocean biogeochemical data product, GLODAPv2. 2021. *Earth System Science Data Discussions*, 1–32.

Lee, S.-K., Lumpkin, R., Baringer, M. O., Meinen, C. S., Goes, M., Dong, S., ... Yeager, S. G. (2019). Global meridional overturning circulation inferred from a data-constrained ocean & sea-ice model. *Geophysical Research Letters*, *46*(3), 1521–1530.

Lehmann, N., Kienast, M., Granger, J., Bourbonnais, A., Altabet, M., & Tremblay, J.-É. (2019). Remote western Arctic nutrients fuel remineralization in deep Baffin Bay. *Global Biogeochemical Cycles*, *33*(6), 649–667.

Le Roy, E., Sanial, V., Charette, M. A., Beek, P. v., Lacan, F., Jacquet, S. H., ... others (2018). The 226 Ra–Ba relationship in the North Atlantic during GEOTRACES-GA01. *Biogeosciences*, *15*(9), 3027–3048.

Mahoney, J., Sinton, J., Kurz, M., Macdougall, J., Spencer, K., & Lugmair, G. (1994). Isotope and trace element characteristics of a super-fast spreading ridge: East Pacific Rise, 13–23°S. *Earth and Planetary Science Letters*, *121*(1-2), 173–193.

Marshall, J., Donohoe, A., Ferreira, D., & McGee, D. (2014). The ocean's role in setting the mean position of the Inter-Tropical Convergence Zone. *Climate Dynamics*, *42*(7), 1967–1979.

McCartney, M. S. (1977). Subantarctic Mode Water. In M. V. Angel (Ed.), *A voyage of discovery: George Deacon 70th anniversary volume* (Supplement to Deep-Sea Research ed., pp. 103–119). Oxford: Pergamon Press.

Measures, C., Henderson, G., Anderson, R., Adkins, J., Andersson, P., Boyle, E., ... Zhang, J. (2007). GEOTRACES–An international study of the global marine biogeochemical cycles of trace elements and their isotopes. *Geochemistry*,

67(2), 85–131.
Mecking, S., & Warner, M. J. (2001). On the subsurface CFC maxima in the subtropical North Pacific thermocline and their relation to mode waters and oxygen maxima. *Journal of Geophysical Research: Oceans*, *106*(C10), 22179–22198.
Miura, T., Suga, T., & Hanawa, K. (2002). Winter mixed layer and formation of dichothermal water in the Bering Sea. *Journal of Oceanography*, *58*(6), 815–823.
Molinelli, E. J. (1981). The Antarctic influence on Antarctic Intermediate Water. *Journal of Marine Research*, *39*, 267–293.
Montes, I., Dewitte, B., Gutknecht, E., Paulmier, A., Dadou, I., Oschlies, A., & Garçon, V. (2014). High-resolution modeling of the Eastern Tropical Pacific oxygen minimum zone: Sensitivity to the tropical oceanic circulation. *Journal of Geophysical Research: Oceans*, *119*(8), 5515–5532.
Musgrave, D. L., Weingartner, T. J., & Royer, T. C. (1992). Circulation and hydrography in the northwestern Gulf of Alaska. *Deep Sea Research Part A. Oceanographic Research Papers*, *39*(9), 1499–1519.
Nameroff, T., Balistrieri, L., & Murray, J. (2002). Suboxic trace metal geochemistry in the eastern tropical North Pacific. *Geochimica et Cosmochimica Acta*, *66*(7), 1139–1158.
Oka, E., & Suga, T. (2005). Differential formation and circulation of North Pacific central mode water. *Journal of Physical Oceanography*, *35*(11), 1997–2011.
Olsen, A., Key, R. M., Van Heuven, S., Lauvset, S. K., Velo, A., Lin, X., … others (2016). The Global Ocean Data Analysis Project version 2 (GLODAPv2)–an internally consistent data product for the world ocean. *Earth System Science Data*, *8*(2), 297–323.
Orsi, A. H., Johnson, G. C., & Bullister, J. L. (1999). Circulation, mixing, and production of Antarctic Bottom Water. *Progress in Oceanography*, *43*(1), 55–109.
Orsi, A. H., Whitworth III, T., & Nowlin Jr, W. D. (1995). On the meridional extent and fronts of the Antarctic Circumpolar Current. *Deep Sea Research Part I: Oceanographic Research Papers*, *42*(5), 641–673.
Östlund, H., & Stuiver, M. (1980). GEOSECS Pacific radiocarbon. *Radiocarbon*, *22*(1), 25–53.
Peters, B. D., Jenkins, W. J., Swift, J. H., German, C. R., Moffett, J. W., Cutter, G. A., … Casciotti, K. L. (2018). Water mass analysis of the 2013 US GEOTRACES eastern Pacific zonal transect (GP16). *Marine Chemistry*, *201*, 6–19.
Peters, B. D., Lam, P. J., & Casciotti, K. L. (2018). Nitrogen and oxygen isotope measurements of nitrate along the US GEOTRACES Eastern Pacific Zonal Transect (GP16) yield insights into nitrate supply, remineralization, and water mass transport. *Marine Chemistry*, *201*, 137–150.
Piola, A. R., & Georgi, D. T. (1982). Circumpolar properties of Antarctic intermediate water and Subantarctic Mode Water. *Deep Sea Research Part A. Oceanographic Research Papers*, *29*(6), 687–711.
Rafter, P. A., DiFiore, P. J., & Sigman, D. M. (2013). Coupled nitrate nitrogen and oxygen isotopes and organic matter remineralization in the Southern and Pacific Oceans. *Journal of Geophysical Research: Oceans*, *118*(10), 4781–4794.
Reed, R., Khen, G., Stabeno, P., & Verkhunov, A. (1993). Water properties and flow over the deep Bering Sea basin, summer 1991. *Deep Sea Research Part I: Oceanographic Research Papers*, *40*(11), 2325-2334. doi: https://doi.org/10.1016/0967-0637(93)90107-E
Reid, J. L. (1965). Intermediate waters of the Pacific Ocean. *The Johns Hopkins Oceanographic Studies*.
Reid, J. L. (1997). On the total geostrophic circulation of the Pacific Ocean: Flow patterns, tracers, and transports. *Progress in Oceanography*, *39*(4), 263–352.

Roshan, S., & Wu, J. (2015). Water mass mixing: The dominant control on the zinc distribution in the North Atlantic Ocean. *Global Biogeochemical Cycles*, *29*(7), 1060–1074.

Royer, T. C. (1979). On the effect of precipitation and runoff on coastal circulation in the Gulf of Alaska. *Journal of Physical Oceanography*, *9*(3), 555–563.

Sarmiento, J. L. (2013). Organic matter export and remineralization. In *Ocean biogeochemical dynamics* (pp. 173–226). Princeton University Press.

Schmitz Jr, W. J. (1996). *On the World Ocean Circulation. Volume 1. Some Global Features/North Atlantic Circulation.* (Tech. Rep. No. WHOI-96-0B). Woods Hole, MA: Woods Hole Oceanographic Institution.

Schroeder, I. D., Santora, J. A., Bograd, S. J., Hazen, E. L., Sakuma, K. M., Moore, A. M., ... Field, J. C. (2019). Source water variability as a driver of rockfish recruitment in the California Current Ecosystem: Implications for climate change and fisheries management. *Canadian Journal of Fisheries and Aquatic Sciences*, *76*(6), 950–960.

SeaDataNet. (2010, May). Data quality control procedures (2.0 ed.) [Computer software manual].

Seckel, G. R. (1968). A time-sequence oceanographic investigation in the North Pacific trade-wind zone. *Eos, Transactions American Geophysical Union*, *49*(1), 377–387.

Sedwick, P. N., McMurtry, G., & Macdougall, J. (1992). Chemistry of hydrothermal solutions from Pele's vents, Loihi Seamount, Hawaii. *Geochimica et Cosmochimica Acta*, *56*(10), 3643–3667.

Shrikumar, A., Lawrence, R., & Casciotti, K. L. (2022). PYOMPA technical note. Retrieved from `essoar.org/doi/10.1002/essoar.10507053.4`

Silva, N., Rojas, N., & Fedele, A. (2009). Water masses in the Humboldt Current System: Properties, distribution, and the nitrate deficit as a chemical water mass tracer for Equatorial Subsurface Water off Chile. *Deep Sea Research Part II: Topical Studies in Oceanography*, *56*(16), 1004–1020.

Sloyan, B. M., & Rintoul, S. R. (2001). Circulation, renewal, and modification of Antarctic Mode and Intermediate Water. *Journal of Physical Oceanography*, *31*(4), 1005–1030.

Sprintall, J., & Tomczak, M. (1993). On the formation of Central Water and thermocline ventilation in the southern hemisphere. *Deep Sea Research Part I: Oceanographic Research Papers*, *40*(4), 827–848.

Stramma, L., Johnson, G. C., Firing, E., & Schmidtko, S. (2010). Eastern Pacific oxygen minimum zones: Supply paths and multidecadal changes. *Journal of Geophysical Research: Oceans*, *115*(C9).

Sverdrup, H. U., Johnson, M. W., Fleming, R. H., et al. (1942). *The oceans: Their physics, chemistry, and general biology* (Vol. 1087). Prentice-Hall New York.

Talley, L. D. (1988). Potential vorticity distribution in the North Pacific. *Journal of Physical Oceanography*, *18*(1), 89–106.

Talley, L. D. (1993). Distribution and formation of North Pacific intermediate water. *Journal of Physical Oceanography*, *23*(3), 517–537.

Talley, L. D. (2011). *Descriptive physical oceanography: An introduction.* Academic Press.

Talley, L. D. (2013). Closure of the global overturning circulation through the Indian, Pacific, and Southern Oceans: Schematics and transports. *Oceanography*, *26*(1), 80–97.

Talley, L. D., & Joyce, T. M. (1992). The double silica maximum in the North Pacific. *Journal of Geophysical Research: Oceans*, *97*(C4), 5465–5480.

Talley, L. D., Joyce, T. M., & Deszoeke, R. A. (1991). Transpacific sections at 47 N and 152 W: distribution of properties. *Deep Sea Research Part A. Oceanographic Research Papers*, *38*, S63–S82.

Talley, L. D., Nagata, Y., Fujimura, M., Iwao, T., Kono, T., Inagake, D., ... Okuda,

K. (1995). North Pacific intermediate water in the Kuroshio/Oyashio mixed water region. *Journal of Physical Oceanography*, *25*(4), 475–501.

Teng, Y.-C., Primeau, F. W., Moore, J. K., Lomas, M. W., & Martiny, A. C. (2014). Global-scale variations of the ratios of carbon to phosphorus in exported marine organic matter. *Nature Geoscience*, *7*(12), 895–898.

Thomson, R. E., & Krassovski, M. V. (2010). Poleward reach of the California Undercurrent extension. *Journal of Geophysical Research: Oceans*, *115*(C9).

Tomczak, M. (1981, January). A multi-parameter extension of temperature/salinity diagram techniques for the analysis of non-isopycnal mixing. *Prog. Oceanogr.*, *10*(3), 147–171.

Tomczak, M., & Godfrey, J. (2003a). Hydrology of the Pacific Ocean. In *Regional oceanography: An introduction* (chap. 9). New Delhi, India: Daya Publishing House.

Tomczak, M., & Godfrey, J. S. (2003b). *Regional oceanography: An introduction.* New Delhi, India: Daya Publishing House.

Tomczak, M., & Liefrink, S. (2005). Interannual variations of water mass volumes in the Southern Ocean. *Journal of Atmospheric & Ocean Science*, *10*(1), 31–42.

Trefry, J. H., Butterfield, D. B., Metz, S., Massoth, G. J., Trocine, R. P., & Feely, R. A. (1994). Trace metals in hydrothermal solutions from Cleft segment on the southern Juan de Fuca Ridge. *Journal of Geophysical Research: Solid Earth*, *99*(B3), 4925–4935.

Tsuchiya, M., & Talley, L. D. (1998). A Pacific hydrographic section at 88°W: Water-property distribution. *Journal of Geophysical Research: Oceans*, *103*(C6), 12899–12918.

Ueno, H., & Yasuda, I. (2000). Distribution and formation of the mesothermal structure (temperature inversions) in the North Pacific subarctic region. *Journal of Geophysical Research: Oceans*, *105*(C7), 16885–16897.

Ueno, H., & Yasuda, I. (2003). Intermediate water circulation in the North Pacific subarctic and northern subtropical regions. *Journal of Geophysical Research: Oceans*, *108*(C11).

Van Scoy, K. A., Olson, D. B., & Fine, R. A. (1991). Ventilation of North Pacific intermediate waters: The role of the Alaskan gyre. *Journal of Geophysical Research: Oceans*, *96*(C9), 16801–16810.

Whitworth III, T., Orsi, A., Kim, S.-J., Nowlin Jr, W., & Locarnini, R. (1985, January). Ocean, ice, and atmosphere: Interactions at the Antarctic continental margin. In S. S. Jacobs & R. F. Weiss (Eds.), (Vol. 75, pp. 1–27). Washington, D.C.: American Geophysical Union. (https://doi.org/10.1029/AR075p0001)

Wyrtki, K. (1967). Circulation and water masses in the eastern equatorial Pacific Ocean. *International Journal of Oceanology & Limnology*, *1*(2), 117–147.

Yamagishi, H., Westley, M. B., Popp, B. N., Toyoda, S., Yoshida, N., Watanabe, S., … Yamanaka, Y. (2007). Role of nitrification and denitrification on the nitrous oxide cycle in the eastern tropical North Pacific and Gulf of California. *Journal of Geophysical Research: Biogeosciences*, *112*(G2).

Yasuda, I. (1997). The origin of the North Pacific intermediate water. *Journal of Geophysical Research: Oceans*, *102*(C1), 893–909.

You, Y., Suginohara, N., Fukasawa, M., Yasuda, I., Kaneko, I., Yoritaka, H., & Kawamiya, M. (2000). Roles of the Okhotsk Sea and Gulf of Alaska in forming the North Pacific intermediate water. *Journal of Geophysical Research: Oceans*, *105*(C2), 3253–3280.

You, Y., Suginohara, N., Fukasawa, M., Yoritaka, H., Mizuno, K., Kashino, Y., & Hartoyo, D. (2003). Transport of North Pacific intermediate water across Japanese WOCE sections. *Journal of Geophysical Research: Oceans*, *108*(C6).

Yuan, X., & Talley, L. D. (1992). Shallow salinity minima in the North Pacific. *Journal of Physical Oceanography*, *22*(11), 1302–1316.